CMS Physics Analysis Summary

Contact: cms-pag-conveners-susy@cern.ch 2012/05/01

Search for Supersymmetry in hadronic final states using M_{T2} with the CMS detector at $\sqrt{s}$ = 7 TeV

The CMS Collaboration

Abstract

A search for Supersymmetry or similar new physics was carried out using a $\sqrt{s} = 7$ TeV pp collisions data sample corresponding to 4.73 fb^{-1}of integrated luminosity collected by the CMS experiment at the LHC. Fully hadronic final states were selected based on the stransverse mass variable M_{T2}. Two complementary analyses were performed. The first targets the region of parameter space with medium to high squark and gluino masses, in which the signal can be separated from the Standard Model backgrounds by a strong cut on M_{T2}. A second analysis has been optimized to look for events with a light gluino but heavy squarks. In this case, the M_{T2} cut was relaxed, but a higher jet multiplicity and at least one b-tagged jet were required. The dominant backgrounds in both analyses are different and they were estimated using data-driven methods. As no excess of events over the expected background was observed, exclusion limits were derived on the parameter space of the constrained minimal supersymmetric extension of the Standard Model (mSUGRA/CMSSM), as well as on a variety of Simplified Model Spectra.

1 Introduction

A search for physics beyond the Standard Model in pp collisions collected by the Compact Muon Solenoid (CMS) detector at the Large Hadron Collider (LHC) at a centre-of-mass energy of 7 TeV is described. The results are based on the full data sample collected in 2011, amounting to 4.73 fb^{-1}of integrated luminosity.

It is well known that a search in a hadronic final state accompanied by large missing transverse momentum ($E_{\mathrm{T}}^{\mathrm{miss}}$) is very sensitive to a broad class of new physics models, including Supersymmetry [1] (SUSY) with R-parity conservation. We present results of a search using the stransverse mass variable, M_{T2} [2, 3], to select new physics candidate events. M_{T2} is the natural extension of the classical transverse mass M_T to the case of supersymmetry where two coloured sparticles are pair-produced and both decay through a cascade of jets and possibly leptons to the Lightest Supersymmetric Particle (LSP). The LSP is not visible in the detector and leads to a missing transverse momentum signature. Although M_{T2} was originally introduced to derive the masses of sparticles involved in the cascade decay, we use it here as a discovery variable which is very sensitive to the presence of new SUSY-like physics. The distribution of M_{T2} reflects the produced particle masses. These are much lighter for the Standard Model background processes than for the SUSY processes. Hence, new physics is expected to show up as an excess in the tail of M_{T2}.

The analysis follows two main directions. A first approach, the "M_{T2} analysis", targets events resulting from heavy sparticle production, characterized by large $E_{\mathrm{T}}^{\mathrm{miss}}$ and large M_{T2}. The Standard Model (SM) backgrounds in the signal region consist of $W(l\nu)$+jets, $Z(\nu\bar{\nu})$+jets and $t\bar{t}$, which are estimated by "data-driven" methods. This analysis is less performant in the case where squarks are heavy and gluinos are light, in which case the production is dominated by gluino-gluino processes. The gluinos give rise to 3-body decays with relatively small $E_{\mathrm{T}}^{\mathrm{miss}}$. Since the gluino decay is mediated by virtual squark exchange and the stop and sbottom are expected to be lighter than the first and second generation squarks, these events can be rich in b-quarks. To increase the sensitivity to such processes, a second approach, the "$M_{T2}b$ analysis", has been designed in which the minimum M_{T2} defining the signal region is lowered. To suppress the QCD background, this lowering is compensated by the requirement of at least one b-tagged jet and a harder cut on the jet multiplicity. We find that this analysis leads to a higher signal to background ratio in the region of heavy squarks and light gluinos and hence improves our sensitivity to this scenario.

This note is organized as follows: after a brief introduction to M_{T2} and its salient properties in Sect. 2, and a summary of the CMS detector in Sect. 3, we describe in Sect. 4 the data samples used and the event selection. In Sect. 5, the search strategy is presented and applied to the M_{T2} analysis in Sect. 6 and to the $M_{T2}b$ analysis in Sect. 7. In these sections the data-driven background estimations are also discussed. As no excess compared to the expectations from SM physics is observed, we proceed with establishing exclusion limits in Sect. 9. Finally, Sect. 10 contains our conclusions.

2 Definition of M_{T2} and interpretation

The variable M_{T2} or stranverse mass was introduced [2] to measure the mass of primary pair-produced particles in a situation where both ultimately decay into undetected particles (e.g. neutralino LSPs) leaving the event kinematics underconstrained. It assumes that the two produced sparticles give rise to identical types of decay chains with two visible systems defined by their transverse momenta, $\vec{p}_T^{\,vis(i)}$, energies $E_T^{vis(i)}$, and masses $m^{vis(i)}$. They are accompanied

by the unknown LSP transverse momenta, $p_T^{\chi(i)}$. In analogy with the transverse mass used for the W mass determination, we can define two transverse masses ($i = 1, 2$)

$$(m_T^{(i)})^2 = (m^{vis(i)})^2 + m_\chi^2 + 2\left(E_T^{vis(i)} E_T^{\chi(i)} - \vec{p}_T^{\,vis(i)} \cdot \vec{p}_T^{\,\chi(i)}\right) \quad (1)$$

These have the property (like for W decay) that for the true LSP mass their distribution cannot exceed the mass of the parent particle of the decay and they present an endpoint at the value of the parent mass. The momenta $p_T^{\chi(i)}$ of the unseen particles are not experimentally accessible individually and only their sum, the missing transverse momentum p_T^{miss}, is known. Therefore, in the context of SUSY, a generalization of the transverse mass is needed and the proposed variable is M_{T2}. It is defined as

$$M_{T2}(m_\chi) = \min_{p_T^{\chi(1)} + p_T^{\chi(2)} = p_T^{miss}} \left[\max\left(m_T^{(1)}, m_T^{(2)}\right)\right], \quad (2)$$

where the LSP mass m_χ remains as a free parameter. This formula can be understood as follows. As neither of $m_T^{(1)}$ nor $m_T^{(2)}$ can exceed the parent mass if the true momenta are used, the larger of the two can be chosen. To make sure that M_{T2} does not exceed the parent mass, a minimization is performed on trial LSP momenta fulfilling the $E_{\mathrm{T}}^{\mathrm{miss}}$ constraint. The distribution of M_{T2} for the correct value of m_χ then has an endpoint at the value of the primary particle mass. If, however, m_χ is lower (higher) than the correct mass value, the endpoint will be below (above) the parent mass. If Initial State Radiation (ISR) can be neglected, an analytic expression for M_{T2} has been computed in [4]. In practice, the determination of M_{T2} may be complicated by the presence of ISR or equivalently transverse momentum from decays occurring upstream in the decay chain (UTM) in case M_{T2} is computed for subsystems [5]. In this case, no analytic expression for M_{T2} is known, but it can be computed numerically, using e.g. the code of [6].

In this note, we attempt to use M_{T2} as a variable to distinguish SUSY production events from SM backgrounds. The use of M_{T2} as a discovery variable was first proposed in [7] , but in this note we follow a different approach. Several choices for the visible system used as input to M_{T2} can be considered: purely dijet events (as in [7]), selecting the two leading jets in multijet events or grouping jets together to form two systems or *pseudojets*.

A method to subdivide multijet events in two pseudojets is the reconstruction of "event hemispheres" described in [8], Sect. 13.4. The hemisphere reconstruction works as follows: first, two initial axes (seeds) are chosen. Here, we take them as the directions of the two massless jets which have the largest invariant mass. Next, the other jets are associated to one of these axes according to the following criterion (hemisphere association method). We used the minimal Lund distance [9], meaning that jet k is associated to the hemisphere with mass m_i rather than m_j if

$$(E_i - p_i cos\theta_{ik})\frac{E_i}{(E_i + E_k)^2} \leq (E_j - p_j cos\theta_{jk})\frac{E_j}{(E_j + E_k)^2}. \quad (3)$$

After all jets are associated to one or the other axis, the axes are recalculated as the sum of the momenta of all jets connected to a hemisphere and the association is iterated using these new axes until no jets switch from one group to the other.

To get a better understanding of the behaviour of M_{T2}, we take the simple example of M_{T2} without ISR nor upstream transverse momentum. It can be seen from the equation for M_{T2} in [4] that the whole angular and p_T dependence of M_{T2} is encoded in a variable A_T

$$A_T = E_T^{vis(1)} E_T^{vis(2)} + \vec{p}_T^{\,vis(1)} \cdot \vec{p}_T^{\,vis(2)} \quad (4)$$

and that M_{T2} increases with increasing A_T. Therefore, the minimum value of M_{T2} is reached in configurations where (pseudo)jets are back-to-back and the maximum when they are parallel to each other and with a large p_T. In the simple case where $m_\chi = 0$ is chosen and the visible systems have zero mass, M_{T2} becomes

$$(M_{T2})^2 = 2A_T = 2p_T^{vis(1)} p_T^{vis(2)}(1 + cos\phi_{12}), \tag{5}$$

where ϕ_{12} is the angle between the two (pseudo)jets in the transverse plane. It is seen that this corresponds to the transverse mass of system 1 with an unseen neutral particle of momentum equal to the momentum of system 2 but opposite to it.

SUSY events with large expected $E_{\mathrm{T}}^{\mathrm{miss}}$ and large acoplanarity will be concentrated in the large M_{T2} region. On the contrary, QCD dijet events, being back-to-back, will populate the region of minimum M_{T2}, regardless of the magnitude of the $E_{\mathrm{T}}^{\mathrm{miss}}$ or jet p_T. M_{T2} is zero for massless (pseudo)jets if we choose $m_\chi = 0$. Hence, M_{T2} has a built-in protection against QCD jet mismeasurements, even if they have a large $E_{\mathrm{T}}^{\mathrm{miss}}$. However, mismeasured QCD multijet events may give rise to pseudojets away from the back-to-back configuration, leading to $M_{T2} > 0$ GeV. For this reason, further protections against $E_{\mathrm{T}}^{\mathrm{miss}}$ from mis-measurements need to be introduced. Furthermore, defining pseudojets as massless may be a good approach towards further suppressing QCD multijet events in the M_{T2} tail. Other backgrounds consist of events containing true $E_{\mathrm{T}}^{\mathrm{miss}}$, as these can lead to (pseudo)jets away from the back-to-back topology. Candidates are $t\bar{t}$ or W+jets with leptonic decays and $Z(\rightarrow \nu\nu)$+jets. In the follwing, M_{T2} is computed for massless pseudojets and $m_\chi = 0$.

3 CMS detector

The central feature of the CMS apparatus is a superconducting solenoid 13m in length and 6m in diameter which provides an axial magnetic field of 3.8 T. The core of the solenoid is instrumented with various particle detection systems. The iron return yoke outside the solenoid is in turn instrumented with gas detectors which are used to identify muons. Charged particle trajectories are measured by the silicon pixel and strip tracker, covering $0 < \phi < 2\pi$ in azimuth and $|\eta| < 2.5$, where the pseudorapidity η is defined as $\eta = -\log\ \tan(\theta/2)$, with θ being the polar angle of the trajectory of the particle with respect to the counter-clockwise beam direction. A lead tungstate crystal electromagnetic calorimeter (ECAL) and a brass-scintillator hadronic calorimeter (HCAL) surround the tracking volume and cover the region $|\eta| < 3$. A quartz-steel Cerenkov-radiation-based forward hadron calorimeter extends the coverage to $|\eta| \leq 5$. The detector is nearly hermetic, allowing for energy balance measurements in the plane transverse to the beam directions. A detailed description of the CMS detector can be found elsewhere [10].

4 Data/MC samples and event selection

The data used in this analysis were collected by triggers based on the quantity H_T, the scalar sum of transverse momenta of reconstructed and energy corrected calorimeter jets with $p_T \geq 40$ GeV. Due to a continuous increase in instantaneous luminosity condition, the trigger evolved with time from a cut $H_T > 440$ GeV to $H_T > 650$ GeV.

The analysis strategy was designed using Monte Carlo simulation (MC). The MC samples were generated with PYTHIA 6.4.22 [9] and MADGRAPH 5 [11], and processed with a detailed simulation of the CMS detector response based on GEANT4 [12]. The events were reconstructed and analyzed in the same way as the data. In the case of SM background MC samples we have

used the most accurate calculation of the cross sections available in the literature, usually at Next-to-Leading-Order (NLO). For the CMS SUSY benchmark signal samples, described in [8] Sect. 13.3 and summarized in Table 1, we used NLO cross sections obtained by weighting the LO cross sections from PYTHIA by sub-process dependent K-factors calculated with Prospino [13].

Table 1: Definition of LM benchmark points, from [8]. For all points, the sign of μ is positive.

Benchmark point	LM6	LM7	LM8	LM9
m_0	85	3000	500	1450
$m_{1/2}$	400	230	300	175
$\tan\beta$	10	10	10	50
A_0	0	0	-300	0
σ(pb), NLO	0.403	1.34	1.03	10.56

Offline, the events are reconstructed in a consistent way using the particle-flow (PF) event description [14], which identifies and reconstructs individually the particles produced in the collision, namely charged hadrons, photons, neutral hadrons, muons, and electrons.

Electrons and muons with $p_T \geq 10$ GeV and $|\eta| \leq 2.4$ are considered isolated if the transverse momentum sum of charged hadrons, photons, and neutral hadrons surrounding the lepton, with $\Delta R = \sqrt{\Delta\eta^2 + \Delta\phi^2} < 0.4$, divided by the lepton transverse momentum itself was less than 0.2. The electron and muon reconstruction and identification are described in refs. [15, 16] and [17] respectively. All particles apart from the isolated electrons and muons were then clustered into jets by the anti-k_{T} jet clustering algorithm [18] with a distance parameter $R = 0.5$ forming particle-flow jets [19, 20]. Jet energies were calibrated by applying correction factors as a function of the transverse momentum and the pseudo-rapidity of the jet. Residual jet energy corrections were applied in the data to bring the jet energy scale to the one observed in the simulation [21]. The effect of pile-up was reduced by using the FastJet pile-up subtraction procedure [22, 23] for data and MC. Jets were required to pass loose quality criteria and have a $p_T \geq 20$ GeV and $|\eta| \leq 2.4$. The missing transverse energy, $E_{\mathrm{T}}^{\mathrm{miss}}$, was computed as the absolute value of the vector sum of all particles reconstructed by the PF algorithm.

Events are required to have at least one good vertex [24]. The triggers were measured to be nearly 100% efficient in the region where events are selected offline with $H_T > 750$ GeV, formed from PF jets, for the full data set used in this analysis. At least three good jets were required, the two leading jets with $p_T \geq 100$ GeV, the third one with $p_T \geq 40$ GeV. The $E_{\mathrm{T}}^{\mathrm{miss}}$ was required to be larger than 30 GeV. Events containing beam background or anomalous calorimeter noise were rejected. Several tests were applied to ensure that the selected events did not contain noise and the was $E_{\mathrm{T}}^{\mathrm{miss}}$ unbiased. In order to reject events with an important contribution of soft and/or forward jets to the momentum imbalance, a maximum difference between the $E_{\mathrm{T}}^{\mathrm{miss}}$ and $H_{\mathrm{T}}^{\mathrm{miss}}$ vectors of 70 GeV was imposed, where the $H_{\mathrm{T}}^{\mathrm{miss}}$ was computed as the vector sum of all selected jets. An event was also rejected if it contained hard jets with $p_T \geq 50$ GeV within $|\eta| < 2.4$ failing the jet identification criteria.

It was argued previously that M_{T2} is protected against jet energy mis-measurements in di-jet events. In multi-jet events such mis-measurement can lead to hemispheres not being back-to-back and hence to larger M_{T2}. To protect against this background, a minimum difference in azimuth ϕ between any selected jet and the $E_{\mathrm{T}}^{\mathrm{miss}}$, $\Delta\phi_{min}(jets, E_{\mathrm{T}}^{\mathrm{miss}}) \geq 0.3$, was required. Finally, events were vetoed if they contained an isolated electron or muon, to suppress the contributions from $W + jets$, $Z + jets$ and $t\bar{t}$ backgrounds.

5 Search strategy

The M_{T2} variable was computed after having applied all cuts outlined in Section 4. We will separately consider the fully hadronic channels with $\geq$ 3 jets and a hard M_{T2} cut (the M_{T2} analysis), mostly sensitive in the region of large squark and gluino masses, and with a relaxed M_{T2} cut complemented by a b-tag and higher jet multiplicity with $\geq$ 4 jets, (the $M_{T2}b$ analysis), increasing the sensitivity to the region of low gluino and high squark masses.

Given the event selection outlined above, we do not expect a significant amount of QCD events to enter the signal regions. Nevertheless, a data-driven method was used to estimate an upper limit on the remaining QCD background in the signal regions. The main backgrounds consisting of $W + jets$, $Z + jets$ and $t\bar{t}$ were also evaluated by means of data-driven methods. A common strategy was applied to both the M_{T2} and $M_{T2}b$ analyses:

- Two regions were defined in H_T, a low H_T region for $750 \leq H_T < 950$ GeV and a high H_T region extending above 950 GeV. In each of these regions, several adjacent bins in M_{T2} were defined, 5 bins for the M_{T2} analysis and 4 bins for the $M_{T2}b$ analysis. The lowest bin in M_{T2} was chosen such that the QCD background remained a small fraction of the total background. For the M_{T2} analysis the lowest bin starts at $M_{T2} = 150$ GeV, and for $M_{T2}b$ the lowest bin starts at $M_{T2} = 125$ GeV.
- Data-driven methods were designed for each of the different background contributions. The numbers of events and their relative systematic uncertainties were computed by means of these methods in each bin of H_T / M_{T2}. The methods were designed such that resulting estimates are largely statistically uncorrelated. The method was first applied to the MC and a validity check was performed. Then, it was applied to the data and compared to the MC prediction.
- The predicted numbers of events for all background components and their uncertainties were summed giving an estimate of the total background yield and its uncertainty in each bin.
- The estimated number of background events for each bin was compared to the number of observed events, and the potential contribution from a SUSY signal was quantified by a statistical method based on a multi-bin profile likelihood described in Sect. 9.

The results were systematically compared to the CMS SUSY benchmark points defined in Table 1.

6 M_{T2} analysis

6.1 Event selection

Figure 1 shows the M_{T2} distribution using an integrated luminosity of 4.73 fb^{-1}. For $M_{T2} <$ 80 GeV the distribution is completely dominated by QCD events. For medium M_{T2} values, the distribution is dominated by $W + jets$ and $Z \to \nu\bar{\nu} + jets$ events with some contribution from $t\bar{t}$, while in the tail of M_{T2} the contribution from top-quark production becomes negligible and $Z \to \nu\bar{\nu}$ together with $W + jets$ dominate. We observe excellent agreement between data and simulation in the core as well as in the tail of the distribution. The white distribution (black dotted line) corresponds to the LM6 signal compared to the MC backgrounds. We see that in presence of a signal, we would expect an excess in the tail of M_{T2}, which is not observed.

The corresponding event yields for data and SM MC, after the full selection and for the various

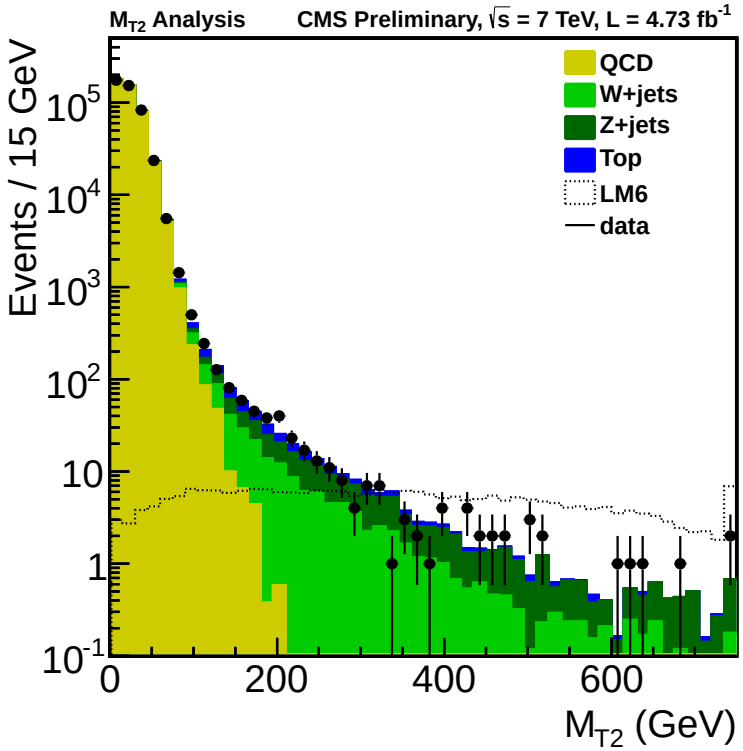

Figure 1: The M_{T2} distribution after having applied all selection cuts and $H_T > 750$ GeV with an integrated luminosity of 4.73 fb^{-1}. The last bin contains the overflow. The different MC backgrounds are stacked on top of each other and normalized to the integrated luminosity. The LM6 signal distribution is normalized to the same integrated luminosity and superposed to the MC background.

bins in M_{T2} are given in Table 2 for the low and the high H_T regions. Contributions from other backgrounds, such as γ+jets, $Z \to ll$ and diboson production, are found to be negligible. It is seen that for all but one M_{T2} bins, the observed number of events in data agree within the uncertainties with the SM background expectations from MC. In the low H_T region, the M_{T2} bin (200, 275] GeV has an excess of data compared to background. We investigated whether the origin could be of instrumental nature, but did not find evidence for it. It could be of statistical origin. The excess has a marginal impact ($< 1\sigma$) on the final observed limit.

6.2 Data-driven background determination

6.2.1 QCD background

From simulation studies, we have determined that the QCD background is negligible in the tail of the M_{T2} distribution. Nevertheless, a data-driven method was designed to verify that this is indeed the case.

We have used a method based on M_{T2} and $\Delta\phi_{min}$, the difference in azimuth between the $E_{\mathrm{T}}^{\mathrm{miss}}$ vector and the closest jet. The background in the signal region, defined by $\Delta\phi_{min} \geq 0.3$ and large M_{T2}, was predicted from a control region with $\Delta\phi_{min} \leq 0.2$. The two variables are strongly correlated, but a factorization method can still be applied if the functional form is known for the ratio of numbers of events $r(M_{T2}) = N(\Delta\phi_{min} \geq 0.3)/N(\Delta\phi_{min} \leq 0.2)$ as a function of M_{T2}. It was found in simulation studies, and confirmed in data, that for $M_{T2} > 50$

Table 2: Expected background event yields and observed number of events in data in the various M_{T2} bins for events with ≥ 3 jets in the low and high H_T regions.

	QCD	W+jets	Top	$Z(\nu\nu)$+jets	total MC	Data
$750 \leq H_T \leq 950$						
All Selections	3.18e+05	9.22e+02	1.30e+03	3.01e+02	3.20e+05	3.20e+05
M_{T2} (150, 200] GeV	3.08	37.5	20.6	27.9	90.0	88
M_{T2} (200, 275] GeV	0.0	20.6	9.40	20.3	50.3	69
M_{T2} (275, 375] GeV	0.0	9.74	2.74	11.6	24.1	19
M_{T2} (375, 500] GeV	0.0	3.63	0.69	6.07	10.4	8
M_{T2} (500, ∞] GeV	0.0	1.54	0.20	3.55	5.29	6
$H_T > 950$						
All Selections	1.22e+05	4.39e+02	6.32e+02	1.42e+02	1.23e+05	1.19e+05
M_{T2} (150, 200] GeV	9.84	19.8	11.7	12.9	54.2	70
M_{T2} (200, 275] GeV	0.47	13.65	5.25	10.50	30.0	23
M_{T2} (275, 375] GeV	0.04	6.43	1.83	6.42	14.7	9
M_{T2} (375, 500] GeV	0.0	1.63	0.40	2.54	4.57	8
M_{T2} (500, ∞] GeV	0.0	1.10	0.16	2.16	3.42	4

GeV the ratio falls off exponentially and, therefore, a parameterization of the form

$$r(M_{T2}) = \frac{N(\Delta\phi_{min} \geq 0.3)}{N(\Delta\phi_{min} \leq 0.2)} = \exp(a - b \cdot M_{T2}) + c \tag{6}$$

has been used for $M_{T2} > 50$ GeV, where the function is assumed to reach a constant value at large M_{T2} due to extreme tails of the jet energy resolution. The fitted parameters were determined from the distribution of QCD simulation events in the high H_T region. It was checked that compatible fit results are obtained when the fit is limited to the region $50 < M_{T2} < 80$ GeV, where the contribution of electroweak and $t\bar{t}$ processes is small. The constant term, however, is only measurable in the signal region when using MC. First, a validation test was performed by estimating the QCD contamination using the predicted events in QCD MC, applying the functional model above. A good agreement was observed. The robustness of the prediction was further checked by varying the fit boundaries and the cut value on $\Delta\phi_{min}$. Next, the fit was repeated on the data in the region $50 < M_{T2} < 80$ GeV after subtracting the electroweak and $t\bar{t}$ contribution (Figure 2). The fitted parameter values are in agreement within uncertainties with the values obtained from the QCD MC. The parameter c was fixed conservatively to the value of the exponential at $M_{T2} = 250$ GeV up to where the agreement with data can be tested. In the lower M_{T2} bins, where the exponential term dominates over the constant term, the QCD prediction from data gives a reliable estimate. For the higher M_{T2} bins, where the constant term dominates, this method overestimates with respect to the MC prediction, nevertheless confirming that the QCD contribution is negligible. The results of the QCD contamination estimates are summarized in Table 3. Finally, the extreme case of the jet energy resolution tail, *i.e.* the total loss of a jet, was studied by selecting high p_T mono-jet events. The total number of events was found to be compatible within the uncertainties with the number expected from the electroweak processes, confirming that the QCD contribution is negligible and hence that the constant c is small.

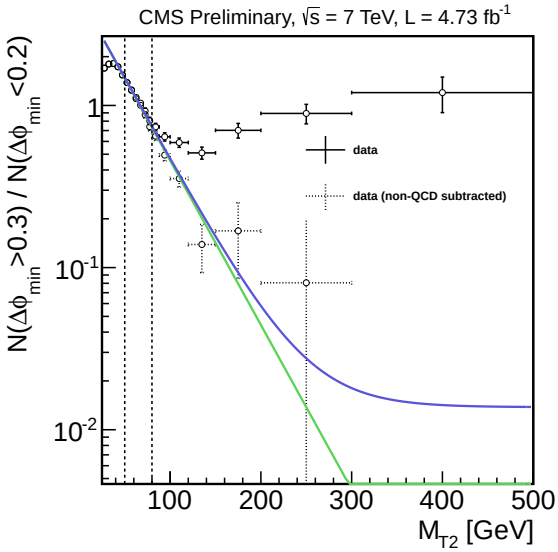

Figure 2: Figure illustrating the QCD estimation method in data. The data shows the ratio $N(\Delta\phi_{min} \geq 0.3)/N(\Delta\phi_{min} \leq 0.2)$ as a function of M_{T2}. The solid points correspond to raw data after all selection cuts, while the dashed points correspond to data after subtracting electroweak and $t\bar{t}$ backgrounds. An exponential fit (green curve) is performed in the region $50 < M_{T2} < 80$ GeV where the non-QCD contribution is minimal. The constant term of the final functional model (blue curve) is taken as the value of the exponential at $M_{T2} = 250$ GeV.

6.2.2 W+jets and $t\bar{t}$ background

The background due to W+jets and semi-leptonic $t\bar{t}$ in the fully hadronic events has the following sources in common:

- leptonic decays of W, where the lepton is unobserved because of the acceptance cuts,
- to a lesser extent, leptonic decays of W, where the lepton is within the acceptance, but fails to satisfy the reconstruction, identification or isolation criteria,
- decays $W \rightarrow \tau\nu_\tau$ where the τ decays hadronically or to a soft lepton failing the acceptance cuts.

The number of events with lost leptons was estimated from the number where a single lepton (e or μ) is found in data and corrected for the probability to lose the lepton, derived from simulation. In Figure 3 we show the M_{T2} for the events with a reconstucted muon. Good agreement between data and MC is observed. To protect against a potential contamination from signal events, a transverse mass cut $M_T < 100$ GeV was introduced. This method was applied in the various H_T and M_{T2} bins. First, a successful validation test of the method was made using MC. Then, a prediction was made from the data bin by bin and found to be in agreement with the MC expectation. The data-driven results are summarized in Table 3. The systematic uncertainty includes the uncertainty on the lepton efficiencies, acceptance and background subtraction.

For the tau contribution, a method similar to the one for lost leptons was used. Events with an isolated and identified hadronically decaying tau [25] were selected in the various H_T and M_{T2} bins. The contribution from fake taus due to jets was subtracted. The remaining number of tau events was corrected for the tau reconstruction and identification efficiency. The agreement between the predicted tau background in data and the one in the MC was checked. Both were found to be compatible and given the small number of events in the data, the numbers of events

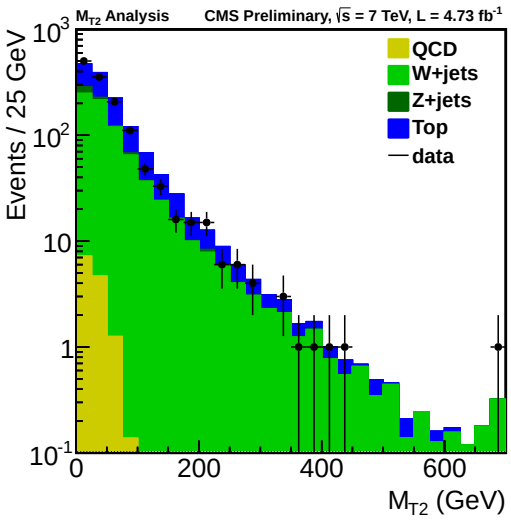

Figure 3: M_{T2} distribution for the events with a reconstructed muon and all selection cuts applied. Good agreement between data and MC is observed.

from the MC are used in Table 3 for the background estimate with the same relative systematic uncertainties as for the lost leptons.

6.2.3 $Z \to \nu\bar{\nu}$ background

The estimate of the $Z \to \nu\bar{\nu}$+jets background was obtained independently from two distinct data samples, one selecting γ + jets events and the other selecting $W \to \mu\nu$ + jets events. In both cases the invisible decay of the Z boson is mimicked by removing, respectively, the photon and the muon from the event, and adding the corresponding p_T to the $E_{\mathrm{T}}^{\mathrm{miss}}$.

6.2.3.1 $Z(\nu\bar{\nu})$+jets from γ+jets. For the estimate using the γ + jets, a sample of events with identified and isolated photons [26] with $p_T > 20$ GeV was selected, where all selection cuts but M_{T2} were imposed. This sample contains both prompt photons as well as π^0s from QCD events. The two components were disentangled by performing a maximum likelihood fit of MC templates to the shower shape separately in the ECAL barrel and endcaps. This event selection is dominated by low p_T photons, where the shower shape provides high discrimination power between prompt photons and π^0s. The extrapolation of their contributions as a function of M_{T2} was obtained from MC. The data to MC comparison of the M_{T2} distribution for the γ+jets events is shown in Figure 4. The $Z \to \nu\bar{\nu}$ background was estimated for each bin in M_{T2} from the number of prompt photon events multiplied by the M_{T2}-dependent ratio of $Z \to \nu\bar{\nu}$ to γ + jets events obtained from MC. This ratio increases as a function of the photon p_T (which drives the M_{T2} value) and reaches a constant value above 300 GeV. The resulting prediction of the background was found to be in excellent agreement with the MC expectation. Systematic uncertainties on the background prediction consist of the statistical uncertainties from the numbers of γ + jets events, a normalization uncertainty in the shower shape fit of 5% and the systematics on the ratio of $Z \to \nu\bar{\nu}$ to γ + jets events due to mis-modeling in the MC. The uncertainties on the ratio were estimated to be less than 20% (30%) for $M_{T2} < 275$ ($M_{T2} > 275$) GeV. They were obtained from the comparison of the photon p_T spectra between the MADGRAPH and JetPhox NLO [27, 28] generators. Additionally, the p_T dependence of the ratio in MC was compared to the one in data by using leptonically decaying Z^0 events and both were found to be in good agreement. This ratio is shown in Figure 4. For $p_T > 400$ GeV this test

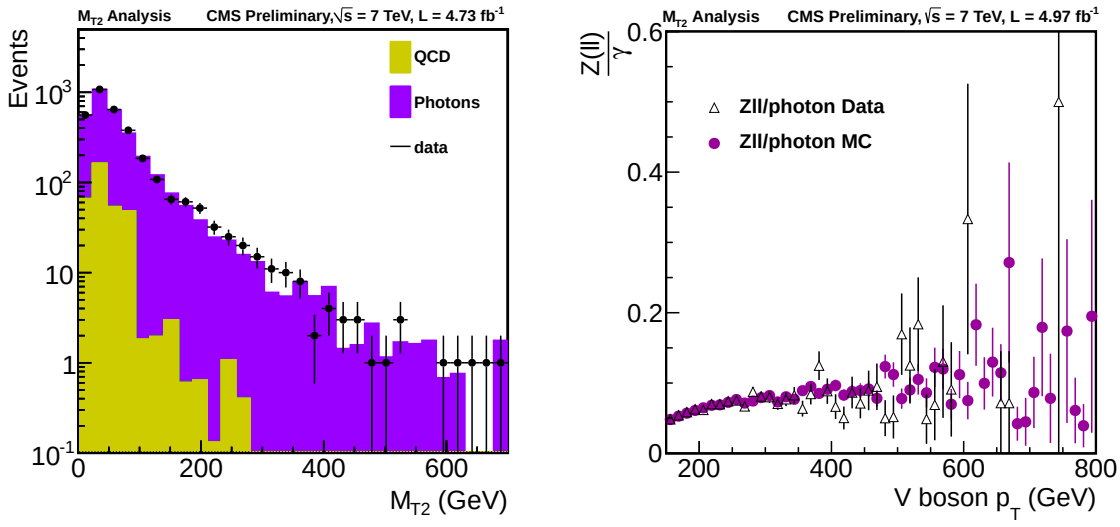

Figure 4: Left: M_{T2} distribution for events with a reconstructed photon, where the photon is added to the $E_{\mathrm{T}}^{\mathrm{miss}}$. Right: $Z^0(e^+e^-, \mu^+\mu^-)$ to photon ratio as a function of the vector boson transverse momentum both for data and MC.

was limited by the statistics of the leptonic Z^0 events, which justifies the increased uncertainty for $M_{T2} > 275$ GeV.

6.2.3.2 $Z(\nu\bar{\nu})$+jets from $W(\mu\nu)$+jets. For the estimate from $W \to \mu\nu$ + jets, corrections are needed for lepton acceptance, lepton reconstruction efficiency and the ratio between W and Z cross sections (including differences in the shape of distributions on which cuts are applied). From the events with a reconstructed muon, a W enriched selection with a reduced $t\bar{t}$ contribution is obtained by applying a b-tag veto. The M_{T2} distribution for these events is shown in Figure 5. The small $t\bar{t}$ contamination to this b-vetoed selection is estimated from data by using

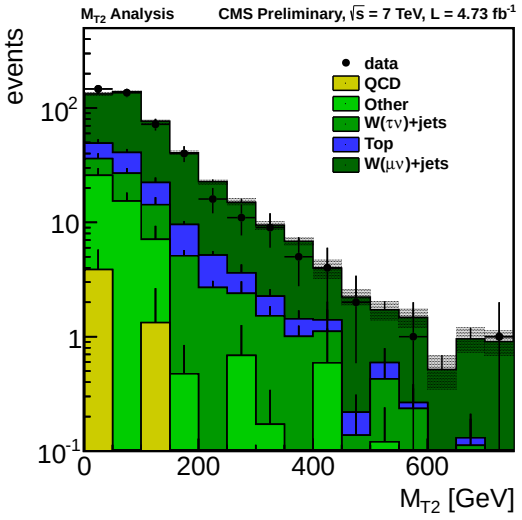

Figure 5: M_{T2} distribution for μ+jets events, where a b-tag veto is used to reduce the $t\bar{t}$ contamination. The muon momentum was added to the $E_{\mathrm{T}}^{\mathrm{miss}}$ to mimic the $Z(\nu\bar{\nu})$ kinematics.

b-tagging to identify the top decay and correcting for the b-tagging efficiency. First, a successful validation test was made using MC events in each of the M_{T2} bins. Secondly, a prediction was

made based on the data in the same M_{T2} bins. Lepton efficiencies were taken from studies of $Z \to \ell^+\ell^-$ events in data. The systematic error includes the uncertainty on the lepton efficiencies, the uncertainty on the b-tagging efficiency from data (used to subtract the $t\bar{t}$ background), the uncertainty on the acceptance from simulation and the uncertainty on the W-to-Z ratio.

The $Z \to \nu\bar{\nu}$ background estimates from $W \to \mu\nu$ + jets and the γ + jets are in good agreement and we have taken the weighted average of the two predictions as the final estimate, since they are statistically uncorrelated. The averaged results are summarized in Table 3.

6.3 Results

The results of the data-driven estimates for the various backgrounds are collected in Table 3 for the low and high H_T regions and are shown in Figure 6.

Table 3: Estimated background event yields in the various M_{T2} and H_T bins. Statistical and systematic uncertainties have been added in quadrature.

	$Z \to \nu\nu$		Lost lepton		$\tau \to had$	QCD		Total bkg.		Data
M_{T2} bin	MC	data pred.	MC	data pred.	Estimate	MC	data pred.	MC	data pred.	
$750 \leq H_T \leq 950$										
[150,200)	27.9	24.2 ± 4.9	36.0	29.6 ± 7.1	22.5 ± 5.4	3.1	7.0 ± 3.5	89.5	83.3 ± 10.7	88
[200,275)	20.3	21.8 ± 4.8	17.2	11.9 ± 3.9	12.7 ± 4.2	0.0	1.0 ± 0.5	50.2	47.4 ± 7.5	69
[275,375)	11.6	13.7 ± 3.8	7.1	4.2 ± 1.9	5.4 ± 2.5	0.0	0.14 ± 0.07	24.1	23.4 ± 4.9	19
[375,500)	6.1	4.1 ± 1.6	2.2	1.1 ± 0.9	2.2 ± 1.8	0.0	0.08 ± 0.05	10.4	7.4 ± 2.6	8
$\geq$500	3.5	1.8 ± 0.9	1.1	1.2 ± 1.0	0.6 ± 0.5	0.0	0.00 ± 0.00	5.3	3.6 ± 1.4	6
$H_T \geq 950$										
[150,200)	12.9	16.7 ± 3.6	18.7	16.2 ± 5.3	12.7 ± 4.1	9.8	11.0 ± 5.5	54.2	56.6 ± 9.4	70
[200,275)	10.5	4.5 ± 2.0	11.7	10.2 ± 3.7	7.1 ± 2.6	0.47	1.4 ± 0.7	29.8	23.2 ± 5.0	23
[275,375)	6.4	5.7 ± 2.2	5.0	2.9 ± 1.7	3.3 ± 1.9	0.04	0.13 ± 0.07	14.7	12.1 ± 3.3	9
[375,500)	2.5	3.0 ± 1.4	1.1	0.6 ± 0.6	0.9 ± 0.9	0.0	0.06 ± 0.04	4.6	4.6 ± 1.8	8
$\geq$500	2.2	2.5 ± 1.5	0.6	0.6 ± 0.6	0.6 ± 0.6	0.0	0.06 ± 0.04	3.4	3.8 ± 1.7	4

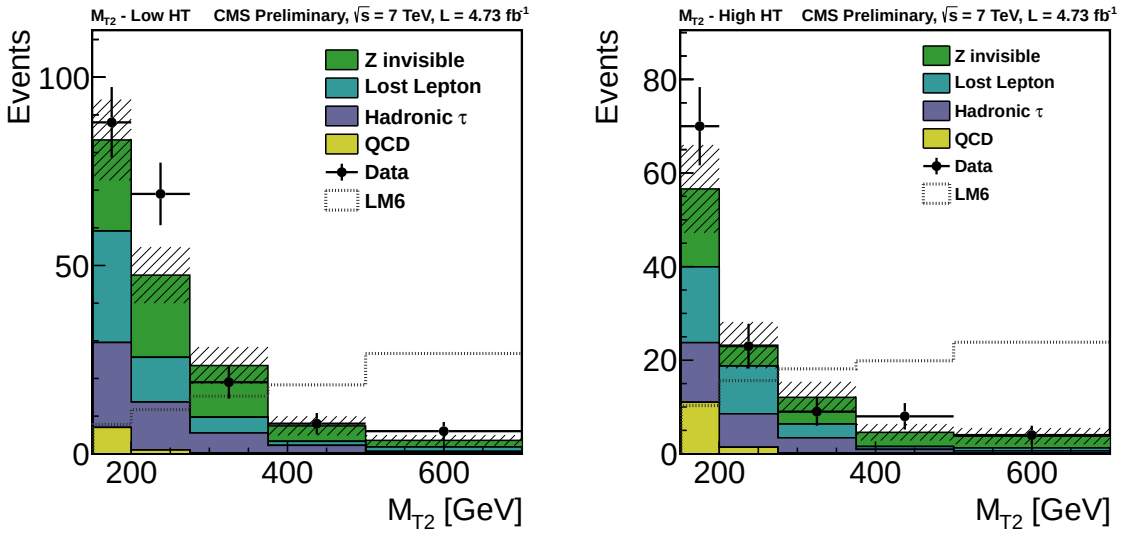

Figure 6: M_{T2} distribution from data-driven background estimates compared to data.

In Table 4 we give the expected event yield for various SUSY benchmark points after the same selection. The events yields were normalized to an integrated luminosity of 4.73 fb^{-1}.

Table 4: Expected signal event yields after various M_{T2} cuts for events with ≥ 3 jets.

	LM6	LM7	LM8	LM9
$750 \leq H_T \leq 950$ GeV				
After Selections	97.9	72.9	188	306
M_{T2} (150, 200] GeV	7.8	9.4	24.0	36.0
M_{T2} (200, 275] GeV	11.7	7.3	26.8	24.8
M_{T2} (275, 375] GeV	15.3	3.5	26.6	10.4
M_{T2} (375, 500] GeV	18.3	0.9	18.7	1.4
M_{T2} (500, ∞) GeV	26.7	0.3	13.2	0.6
$H_T > 950$ GeV				
After Selections	114	62.7	232	235
M_{T2} (150, 200] GeV	10.3	8.0	31.5	25.3
M_{T2} (200, 275] GeV	15.6	7.0	36.1	20.7
M_{T2} (275, 375] GeV	18.2	3.1	30.3	7.8
M_{T2} (375, 500] GeV	19.9	1.0	21.0	4.6
M_{T2} (500, ∞) GeV	23.9	0.1	12.1	3.1

As can be observed from Table 4, the signal efficiency is quite high for several of the benchmark points. However, it is very low for points like LM9 and LM7, showing that the present analysis is not well suited for a search in the region of low $m_{1/2}$ and large m_0.

7 $M_{T2}b$ analysis

7.1 Event selection

It was seen that the M_{T2} analysis provides a powerful means of searching for SUSY signals, especially in the region of large squark and gluino masses. However, the cuts are not optimal for events with heavy squarks and light gluinos, like point LM9. Therefore, somewhat relaxed M_{T2} cuts have been designed to increase the sensitivity to this region. The cut on M_{T2} is reduced to $M_{T2} \geq 125$ GeV and the cut $\Delta\phi(jets, E_{\mathrm{T}}^{\mathrm{miss}}) > 0.3$ is applied to only the four leading jets since a higher jet multiplicity is expected in this region. To suppress the increased QCD background, these cuts are compensated by ≥ 1 b-tag and a larger number of jets, $N_{jets} \geq 4$ for jets with $p_T > 40$ GeV. Also the minimum p_T of the leading jet is required to be at least 150 GeV.

In Figure 7, the M_{T2} distribution is displayed for events satisfying all $M_{T2}b$ analysis cuts and with $H_T > 750$ GeV. The b-tagging is based on the Simple Secondary Vertex (SSV) algorithm [29] where a high purity working point was chosen. This working point has a typical jet tagging efficiency of approximately 42% for b-jets in our search region while the mistagging efficiency for light ($udsg$) jets is of the order of 0.1% and 6.3% for c-jets. The QCD contribution is completely dominant for $M_{T2} \leq 80$ GeV while it is strongly suppressed in the signal region with $M_{T2} \geq 125$ GeV, and the $t\bar{t}$ contribution dominates over the electroweak ones. The white distribution (black dotted line) corresponds to the LM9 signal compared to the MC backgrounds. It is seen that in presence of a signal, we would expect an excess in the tail as well as in the intermediate range of the M_{T2} distribution.

The event yields for data and SM MC are summarized in Table 5 for the low and high H_T regions. It is seen that for all cuts on M_{T2} the agreement between data and MC is good.

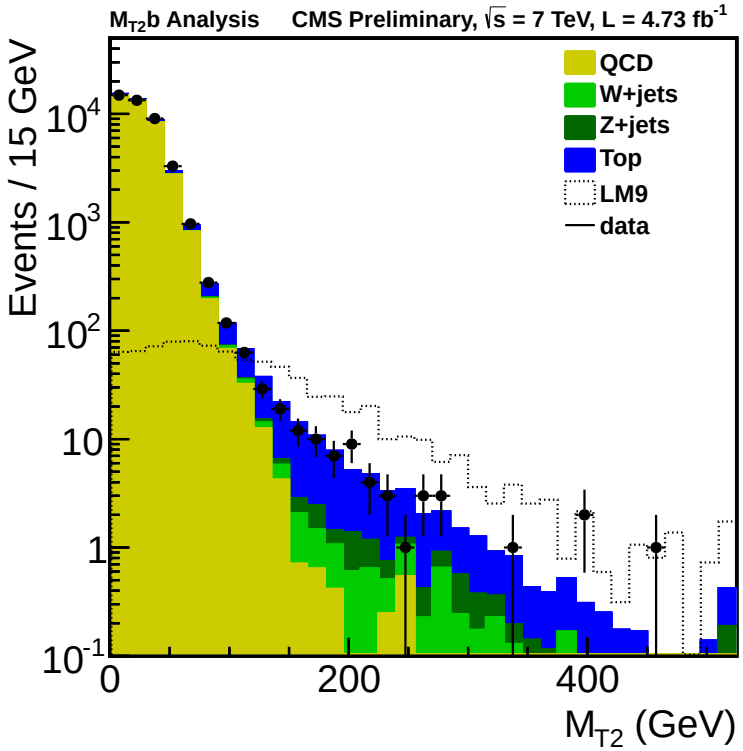

Figure 7: M_{T2} for events including at least one b-tagged jet after having applied all $M_{T2}b$ selection cuts and $H_T > 750$ GeV for an integrated luminosity of 4.73 fb^{-1}. The last bin contains the overflow. The different MC backgrounds are stacked on top of each other and normalized to the integrated luminosity. The LM9 signal distribution is normalized to the same integrated luminosity and superposed to the MC background.

Table 5: Expected background event yields and observed number of events in data after preselection for events with at least one b-tagged jet in the low and high H_T regions.

	QCD	W+jets	Top	$Z(\nu\nu)$+jets	total MC	Data
$750 \leq H_T \leq 950$						
All Selections	2.83e+04	4.53e+02	1.15e+03	1.41e+02	2.97e+04	2.99e+04
M_{T2} (125, 150] GeV	5.16	1.86	20.3	0.95	28.3	22
M_{T2} (150, 200] GeV	0.16	1.94	17.9	2.00	22.1	16
M_{T2} (200, 300] GeV	0.0	1.84	9.43	1.25	12.6	16
M_{T2} (300, ∞] GeV	0.0	0.57	2.55	0.53	3.65	2
$H_T > 950$						
All Selections	1.19e+04	2.18e+01	5.46e+02	6.51e+00	1.25e+04	1.23e+04
M_{T2} (125, 150] GeV	1.25	0.76	9.95	0.64	12.7	10
M_{T2} (150, 180] GeV	0.57	0.79	7.15	0.43	8.96	10
M_{T2} (180, 260] GeV	0.67	1.09	6.62	0.68	9.06	9
M_{T2} (260, ∞] GeV	0.04	0.76	3.09	0.65	4.55	3

7.2 Data-driven background determination

7.2.1 QCD background

Although it is known from simulation that the QCD background is negligible in tail of the M_{T2} distribution, a data-driven estimate has been made to confirm it. The QCD contribution was estimated following the same approach as for the M_{T2} analysis. The function in equation (6) fitted in the region of 50 to 80 GeV gave a satisfactory representation of the QCD distribution. The same fit was subsequently applied to data in the range $50 < M_{T2} < 80$ GeV. From this, the background in the various M_{T2} bins was estimated for the low (high) H_T regions, assuming a constant ratio above $M_{T2} > 250$ GeV. The results are summarized in Table 6.

7.2.2 W+jets and $t\bar{t}$ background

The $t\bar{t}$ background contribution, which dominates, consists in the signal region of $\sim 2/3$ of semi-leptonic decays where the lepton is lost due to the acceptance cuts, reconstruction efficiency or isolation and of $\sim 1/3$ of hadronic tau decays. Their contribution has been evaluated, together with the one from $W + jets$, in the same way as for the M_{T2} analysis, using single electron and single muon events as well as taus decaying to hadrons. The results are summarized in Table 6.

7.2.3 $Z \to \nu\bar{\nu}$ background

The background from events with $Z \to \nu\bar{\nu} + jets$ is very small compared to the $t\bar{t}$. It has been estimated by the same method as for the M_{T2} Analysis, based on $W + jets$ events. A difference is, however, that as the W selection includes a b-veto, to suppress $t\bar{t}$, a ratio of efficiencies for W-events with b-tag over W events without b-tag needs to be taken into account. This ratio is obtained from simulation. The results are summarized in Table 6.

7.3 Results

The results of the data-driven estimates for the various backgrounds are collected in Table 6 for the low and high H_T regions and are shown in Figure 8.

Table 6: Estimated background event yields in the various M_{T2} and H_T bins. The uncertainties are the quadratic sum of statistical and systematic uncertainties.

	$Z \to \nu\nu$		Lost lepton		$\tau \to had$	QCD		Total bkg.		Data
M_{T2} bin	MC	data pred.	MC	data pred.	Estimate	MC	data pred.	MC	data pred.	
$750 \leq H_T \leq 950$										
[125,150)	1.0	0.5 ± 0.4	12.8	4.5 ± 3.2	8.7 ± 6.3	5.16	4.1 ± 2.1	28.3	17.8 ± 7.3	22
[150,200)	2.0	0.7 ± 0.3	11.3	7.6 ± 3.6	8.0 ± 3.8	0.16	0.90 ± 0.51	22.1	17.2 ± 5.2	16
[200,300)	1.3	1.0 ± 0.5	6.1	1.3 ± 1.7	4.9 ± 6.7	0.0	0.04 ± 0.03	12.6	7.2 ± 6.9	16
≥ 300	0.5	0.6 ± 0.3	1.3	1.3 ± 0.9	1.8 ± 1.3	0.0	0.00 ± 0.00	3.7	3.7 ± 1.6	2
$H_T \geq 950$										
[125,150)	0.6	0.4 ± 0.3	6.2	5.9 ± 3.3	4.3 ± 2.4	1.25	5.4 ± 2.8	12.7	16.0 ± 4.9	10
[150,180)	0.4	0.9 ± 0.4	4.6	6.4 ± 3.3	3.2 ± 1.7	0.57	1.7 ± 0.9	9.0	12.2 ± 3.9	10
[180,260)	0.6	0.1 ± 0.1	4.2	3.4 ± 2.3	3.3 ± 2.3	0.67	0.45 ± 0.25	9.1	7.2 ± 3.2	9
≥ 260	0.6	0.7 ± 0.4	2.2	2.0 ± 1.6	1.6 ± 1.3	0.04	0.05 ± 0.04	4.6	4.3 ± 2.0	3

The expected event yield for various SUSY benchmark points is shown in Table 7 after the same selection. The events yields were normalized to an integrated luminosity of 4.73 fb^{-1}. Again, the expected signal for benchmark points could be observable. But more remarkable is

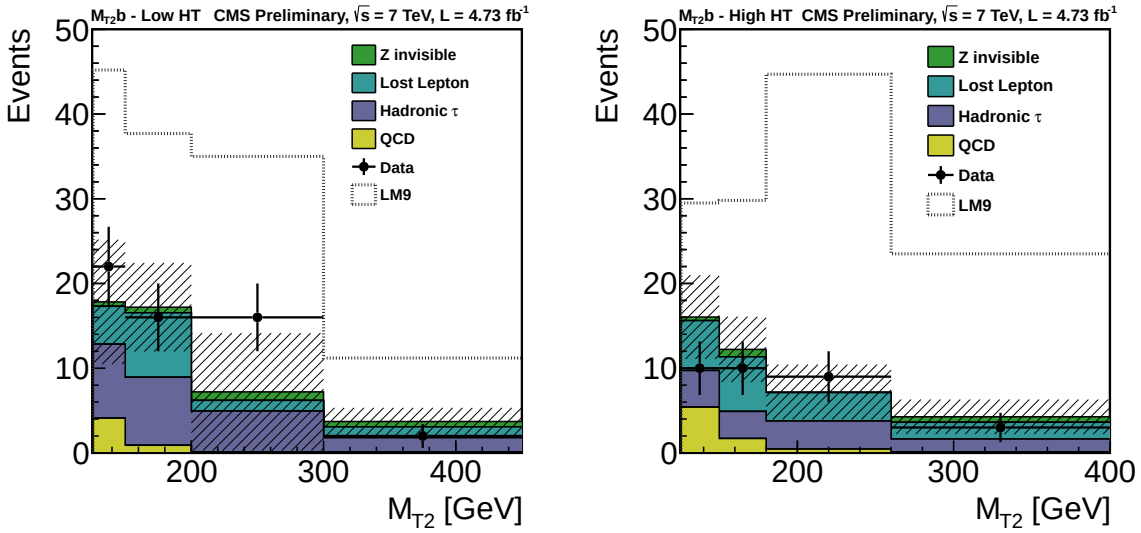

Figure 8: $M_{T2}b$ distribution from data-driven background estimates compared to data. The LM9 histogram is superposed to (and not stacked on top of) the other histograms.

Table 7: Expected signal event yields after various M_{T2} cuts for events with relaxed cuts and at least one b-tagged jet.

	LM6	LM7	LM8	LM9
$750 \leq H_T \leq 950$ GeV				
All Selections	17.5	71.8	269	423
M_{T2} (125, 150] GeV	1.0	5.8	20.1	45.2
M_{T2} (150, 200] GeV	1.7	8.3	33.6	37.7
M_{T2} (200, 300] GeV	3.4	5.9	44.3	35.0
M_{T2} (300, ∞] GeV	7.7	2.7	37.2	11.2
$H_T > 950$ GeV				
All Selections	25.3	72.2	402	373
M_{T2} (125, 150] GeV	1.4	6.0	31.4	29.5
M_{T2} (150, 180] GeV	1.6	4.7	32.6	29.8
M_{T2} (180, 260] GeV	3.9	7.4	61.2	44.7
M_{T2} (260, ∞] GeV	12.1	4.0	71.3	23.5

the increase in efficiency compared to the M_{T2} analysis for points LM7 and LM9, showing that the M_{T2}b analysis cuts indeed increase our sensitivity to the region of heavy squarks and light gluinos.

8 Statistical Interpretation of the results

As no excess is observed upper limits are set on a potential signal. A test on the background-only and signal+background hypotheses is performed using a modified frequentist approach often referred to as CL_s [30].

The contents of the low signal-to-background bins are important for the proper interpretation of the high signal-to-background bins. Simultaneous use of all bins' contents, comparing the observations to the predictions, is needed to optimally compute the significance. For this rea-

son, a multi-bin approach was used in the analysis.

A likelihood function is constructed as the product of Poisson probabilities for each bin of H_T / M_{T2}. The Poisson probabilities are functions of the number of observed events in each bin n_i and the predictions in each bin λ_i, where i ranges from 1 to the number of bins, N_{bins}. The likelihood function is given by

$$\mathcal{L} = \prod_{i=1}^{N_{\text{bins}}} \frac{\lambda_i^{n_i} e^{-\lambda_i}}{n_i!}. \tag{7}$$

The prediction in each bin is a sum over signal and background contributions:

$$\lambda_i = \mu \cdot s_i + \sum_{j=1}^{N_{\text{bkg}}} b_{ij}, \tag{8}$$

where b_{ij} is the background prediction in bin i for background source j, s_i is the signal prediction in bin i, scaled by the *signal strength modifier* μ to test other values of the signal production cross section.

The uncertainties are handled by introducing nuisance parameters θ. The signal and background expectations, therefore, become dependent on N_{syst} nuisance parameters θ_m where $m = 1 \ldots N_{syst}$: $s(\theta_m)$ and $b(\theta_m)$. All sources of uncertainties are taken to be either 100%-correlated (positively or negatively) or uncorrelated (independent), whichever is believed to be appropriate or more conservative. Incorporating the nuisance parameters, the likelihood function becomes:

$$\mathcal{L}(\text{data}|\mu, \theta) = \text{Poisson}(\mu \cdot s(\theta) + b(\theta)) \cdot p(\theta), \tag{9}$$

where $p(\theta)$ is the probability density function (pdf) associated to the given systematic uncertainty. Lognormal pdfs are assumed, a more suitable alternative than the truncated Gaussian in order to describe positively defined parameters. They are characterized by parameter $\kappa = 1 + \epsilon$, where ϵ represents the relative uncertainty for a Gaussian distribution.

In order to compare the compatibility of the data with the background-only and the signal+background hypotheses we construct the test statistic q_μ [31] based on the profile likelihood ratio:

$$q_\mu = -2 \ln \frac{\mathcal{L}(\text{data}|\mu, \hat{\theta}_\mu)}{\mathcal{L}(\text{data}|\hat{\mu}, \hat{\theta})}, \qquad \text{with } 0 \leq \hat{\mu} \leq \mu \tag{10}$$

where "data" can be the actual data observation or pseudo-data. Both the denominator and the numerator are maximized. In the numerator, the signal parameter strength μ remains fixed and the likelihood is maximized for only the nuisance parameters which values at the maximum is denoted as $\hat{\theta}_\mu$. In the denominator, the likelihood is maximized for both μ and θ and $\hat{\mu}$ and $\hat{\theta}$ are the values at which $\mathcal{L}$ reaches its global maximum. The lower constraint $0 \leq \hat{\mu}$ is imposed as the signal strength cannot be negative, while the upper constraint guarantees a one-sided confidence interval (physics-wise, this means that upward fluctuations of data are not considered as evidence against the signal hypothesis). The value of the test for the actual observation is denoted as q_μ^{obs}. This test statistic, defined by the LHC Higgs Combination group [32], differs from what has been used at LEP and Tevatron.

For the limit setting, a modified frequentist CL_s approach is used. Probabilities, or p-values, of observing an outcome of an experiment at least as signal-like as the one observed are calculated for the null (background-only) hypothesis H_0 and for the test (signal+background) hypothesis

H_1:

$$\begin{aligned} CL_{s+b} &= P(q_\mu \geq q_\mu^{obs} | H_1), \\ CL_b &= P(q_\mu \geq q_\mu^{obs} | H_0). \end{aligned} \tag{11}$$

The CL_s quantity is then defined as the ratio of these probabilities:

$$CL_s = \frac{CL_{s+b}}{CL_b}. \tag{12}$$

In the modified frequentist approach, the value CL_s is required to be less than or equal to α in order to declare a $(1-\alpha)$ C.L. exclusion.

In practice, the p-values of the background-only and the signal+background hypotheses are determined from distributions of the test-statistic constructed from simulated pseudo-experiments. Once the ensembles of pseudo-experiments for the two hypotheses are generated, the observed CL_s limit is calculated from these distributions and the actual observation of the test-statistic q_μ^{obs}. The expected CL_s limit is calculated by replacing q_μ^{obs} by the expected median from the distribution of the background-only hypothesis. The limits are computed following the LHC Higgs Combination prescription [32] .

9 Exclusion limits

After taking the systematic uncertainties into account, a 95% upper limit on the number of events has been computed using the CL_s formulation described in Sect. 8. The method determines the fraction, μ, of the signal within the acceptance which is excluded. A resulting fraction $\mu \leq 1$ implies that the tested signal is excluded.

9.1 Exclusion limits in the mSUGRA plane

Exclusion limits at 95% C.L. have been determined in the mSUGRA/CMSSM $(m_0, m_{1/2})$ plane. At each point in the scan four CL_s values are computed for $\mu = 1$ (at NLO): the observed, the median expected, and the $\pm\sigma$ expected edges. If the corresponding CL_s value is smaller than 0.05 the point is excluded at 95% C.L., resulting in the exclusion limits shown in Figure 9 for $A_0 = 0$, $\mu > 0$ and $\tan\beta = 10$. The results from both the M_{T2} and $M_{T2}b$ selections are

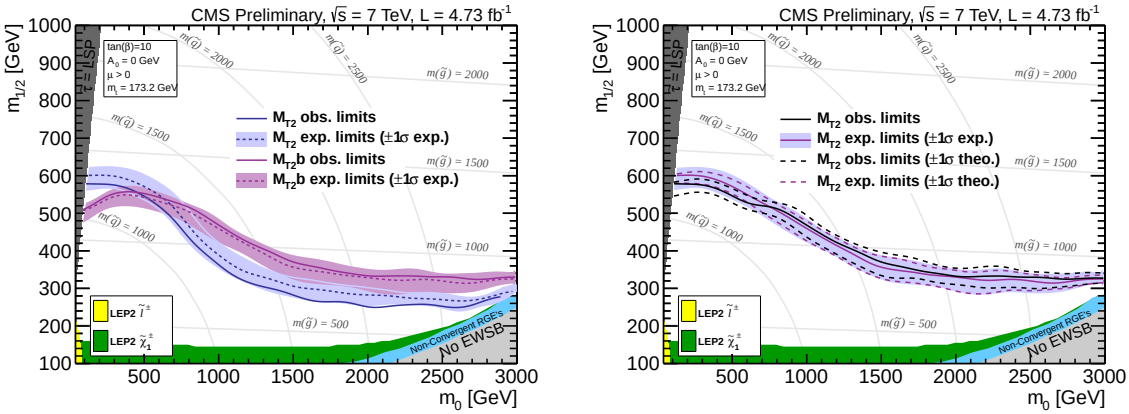

Figure 9: Left: exclusion limit in the mSUGRA/CMSSM $(m_0, m_{1/2})$ plane for the M_{T2} and $M_{T2}b$ analyses with $\tan\beta = 10$. Right: Combined limit based on the best expected limit in each point.

combined based on the best expected limit in each point. The following sources of systematic

uncertainties on the signal yield have been considered: the factorization and renormalization scale, the parton density functions, the jet energy scale and the b-tagging efficiency (in the case of the $M_{T2}b$ analysis). The effect of signal contamination in the leptonic control region (used to estimate the lost lepton background) could be significant and has been taken into account in the limit setting by propagating the signal contribution in the lost lepton control region to the hadronic signal region and subtracting its effect. The exclusion confirms that the M_{T2} analysis is powerful for a search in the region of high squark and gluino masses, i.e. small m_0 and large $m_{1/2}$, whereas the $M_{T2}b$ analysis extends this sensitivity to large squark and small gluino masses, i.e. large m_0 and small $m_{1/2}$.

From these excluded regions, ignoring theory uncertainties, we can derive absolute lower limits on the masses $m(\tilde{\mathrm{q}}) > 1190$ GeV and $m(\tilde{\mathrm{g}}) > 860$ GeV, as well as a limit $m(\tilde{\mathrm{q}}) = m(\tilde{\mathrm{g}}) > 1260$ GeV assuming equal squark and gluino masses. Conservatively, using the -1σ theory uncertainty values, these limits become $m(\tilde{\mathrm{q}}) > 1110$ GeV and $m(\tilde{\mathrm{g}}) > 800$ GeV, and a limit $m(\tilde{\mathrm{q}}) = m(\tilde{\mathrm{g}}) > 1180$ GeV assuming equal squark and gluino masses.

9.2 Exclusion limits in Simplified Models

In this section we interpret the results of our search in terms of Simplified Models [33], which allows to compare the exclusion potential in the context of a larger variety of fundamental models, not necessarily in the MSSM framework. We studied the following topologies:

- Gluino pair production, with $\tilde{g} \to qq\chi^0$
- Gluino pair production, with $\tilde{g} \to bb\chi^0$
- Gluino pair production, with $\tilde{g} \to qqZ\chi^0$

In Fig.10 the 95% C.L. excluded cross sections and mass are reported as a function of the relevant masses for gluino pair production with $\tilde{g} \to qq\chi^0$ using the M_{T2} analysis, and for gluino pair production with $\tilde{g} \to bb\chi^0$ and $\tilde{g} \to qqZ\chi^0$ using the $M_{T2}b$ analysis. Systematic uncertainties on jet energy scale and on b-tagging efficiencies are taken into account as nuisance parameters on the signal model. Exclusion limit curves are derived for the nominal signal cross section (solid lines) as well as for the 3-times (dotted line) and 1/3-times (dashed line) the nominal cross section computed with Prospino [13].

10 Conclusion

We conduct a search for supersymmetry in hadronic final states using the M_{T2} variable calculated from massless pseudojets. M_{T2} is strongly correlated with $E_{\mathrm{T}}^{\mathrm{miss}}$ for SUSY processes, yet provides a natural suppression of QCD backgrounds. A data set containing 4.73 fb^{-1}of integrated luminosity in $\sqrt{s} = 7$ TeV pp collisions taken with the CMS detector during the 2011 LHC run was analyzed. All candidate events were selected using hadronic triggers. Two complementary analyses were performed. The M_{T2} analysis targets decays of moderately heavy squarks and gluinos which naturally feature a sizeable $E_{\mathrm{T}}^{\mathrm{miss}}$. The analysis was based on events containing at least three jets and isolated leptons were vetoed to suppress electroweak processes and $t\bar{t}$ production. We have shown that the tail of the M_{T2} distribution, obtained after this selection, is very sensitive to a potential SUSY signal. A second line of approach, the $M_{T2}b$ analysis, was designed to increase the sensitivity to events with heavy squarks and light gluinos, in which the $E_{\mathrm{T}}^{\mathrm{miss}}$ tends to be smaller. Therefore, the cut on M_{T2} was relaxed and compensated by requiring at least one b-tagged jet and a larger jet multiplicity to suppress the QCD background. For both analyses, the Standard Model backgrounds, arising from QCD multijet, electroweak processes and $t\bar{t}$ production, are obtained through data-

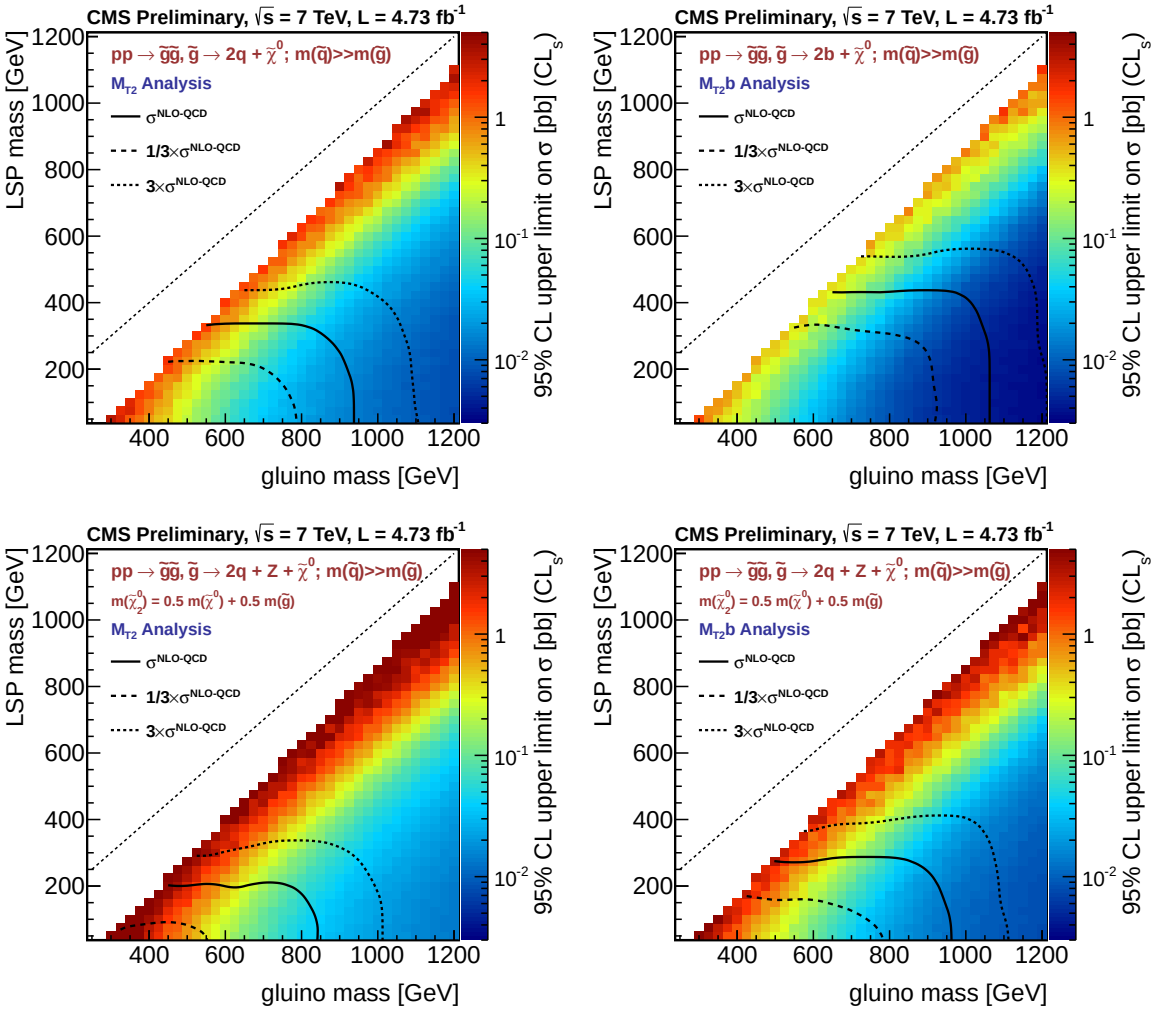

Figure 10: Exclusion limits for Simplified Models. Upper left: gluino pair production with $\tilde{g} \to qq\chi^0$ using the M_{T2} analysis. Upper right: gluino pair production with $\tilde{g} \to bb\chi^0$, using the $M_{T2}b$ analysis. Lower left: gluino pair production with $\tilde{g} \to qqZ\chi^0$, using the M_{T2} analysis. Lower right: gluino pair production with $\tilde{g} \to qqZ\chi^0$, using the $M_{T2}b$ analysis.

driven techniques. No excess beyond the Standard Model expectations has been found; the agreement between the data and the Standard Model predictions is very good both for the M_{T2} and the $M_{T2}b$ analysis. As no evidence for a signal was found, exclusion limits were established in the mSUGRA/CMSSM parameter space, as well as in some simplified models. In the mSUGRA/CMSSM scenario, not including theory uncertainties, an absolute mass limit is obtained for $\tan\beta = 10$ of $m(\tilde{q}) > 1190$ GeV and $m(\tilde{g}) > 860$ GeV, as well as a limit $m(\tilde{q}) = m(\tilde{g}) > 1260$ GeV assuming equal squark and gluino masses. Conservatively, using the -1σ theory uncertainty values, these limits become $m(\tilde{q}) > 1110$ GeV and $m(\tilde{g}) > 800$ GeV, and a limit $m(\tilde{q}) = m(\tilde{g}) > 1180$ GeV assuming equal squark and gluino masses.

References

[1] S. P. Martin, "A Supersymmetry Primer", arXiv:hep-ph/9709356.

[2] C. G. Lester and D. J. Summers, "Measuring masses of semi-invisibly decaying particles pair produced at hadron colliders", *Phys. Lett.* **B463** (1999) 99–103, doi:10.1016/S0370-2693(99)00945-4, arXiv:hep-ph/9906349.

[3] A. Barr, C. Lester, and P. Stephens, "m(T2) : The Truth behind the glamour", *J. Phys.* **G29** (2003) 2343–2363, doi:10.1088/0954-3899/29/10/304, arXiv:hep-ph/0304226.

[4] W. S. Cho, K. Choi, Y. G. Kim et al., "Measuring superparticle masses at hadron collider using the transverse mass kink", *JHEP* **02** (2008) 035, doi:10.1088/1126-6708/2008/02/035, arXiv:0711.4526.

[5] M. Burns, K. Kong, K. T. Matchev et al., "Using Subsystem MT2 for Complete Mass Determinations in Decay Chains with Missing Energy at Hadron Colliders", *JHEP* **03** (2009) 143, doi:10.1088/1126-6708/2009/03/143, arXiv:0810.5576.

[6] H.-C. Cheng and Z. Han, "Minimal Kinematic Constraints and MT2", *JHEP* **12** (2008) 063, doi:10.1088/1126-6708/2008/12/063, arXiv:0810.5178.

[7] A. J. Barr and C. Gwenlan, "The race for supersymmetry: using mT2 for discovery", *Phys. Rev.* **D80** (2009) 074007, doi:10.1103/PhysRevD.80.074007, arXiv:0907.2713.

[8] CMS Collaboration, "CMS technical design report, volume II: Physics performance", *J. Phys. G* **34** (2007) 995–1579, doi:10.1088/0954-3899/34/6/S01.

[9] T. Sjostrand, S. Mrenna, and P. Z. Skands, "PYTHIA 6.4 Physics and Manual", *JHEP* **05** (2006) 026, doi:10.1088/1126-6708/2006/05/026, arXiv:hep-ph/0603175.

[10] CMS Collaboration, "The CMS experiment at the CERN LHC", *JINST* **3** (2008) S08004, doi:10.1088/1748-0221/3/08/S08004.

[11] J. Alwall, M. Herquet, F. Maltoni et al., "MadGraph 5 : Going Beyond", *JHEP* **1106** (2011) 128, doi:10.1007/JHEP06(2011)128, arXiv:1106.0522. * Temporary entry *.

[12] GEANT4 Collaboration, "GEANT4: A simulation toolkit", *Nucl. Instrum. Meth.* **A506** (2003) 250–303, doi:10.1016/S0168-9002(03)01368-8.

[13] W. Beenakker, R. Hopker, and M. Spira, "PROSPINO: A program for the PROduction of Supersymmetric Particles In Next-to-leading Order QCD", arXiv:hep-ph/9611232.

[14] CMS Collaboration, "Particle Flow Event Reconstruction in CMS and Performance for Jets, Taus and MET", *CMS PAS* **PFT-09-001** (2009).

[15] CMS Collaboration, "Electron reconstruction and identication at $\sqrt{s}$ = 7 TeV", *CMS-PAS* **EGM-10-004** (2010).

[16] CMS Collaboration, "Particle-flow commissioning with muons and electrons from J/Psi and W events at 7 TeV", *CMS-PAS* **PFT-10-003** (2010).

[17] CMS Collaboration, "Performance of CMS muon reconstruction in pp collision events at $\sqrt{s}$ = 7 TeV", *CMS-PAS* **MUO-10-004** (2011).

[18] M. Cacciari, G. P. Salam, and G. Soyez, "The anti-k_t jet clustering algorithm", *JHEP* **04** (2008) 063, doi:10.1088/1126-6708/2008/04/063, arXiv:0802.1189.

[19] CMS Collaboration, "Jet Performance in pp Collisions at sqrts=7 TeV", *CMS Physics Analysis Summary* **CMS-PAS-JME-10-003** (2010).

[20] CMS Collaboration, "Commissioning of the Particle-Flow reconstruction in Minimum-Bias and Jet Events from pp Collisions at 7 TeV", *CMS-PAS* **PFT-10-002** (2010).

[21] CMS Collaboration Collaboration, "Determination of Jet Energy Calibration and Transverse Momentum Resolution in CMS", *JINST* **6** (2011) P11002, doi:10.1088/1748-0221/6/11/P11002, arXiv:1107.4277.

[22] M. Cacciari and G. P. Salam, "Pileup subtraction using jet areas", *Phys.Lett.* **B659** (2008) 119–126, doi:10.1016/j.physletb.2007.09.077, arXiv:0707.1378.

[23] M. Cacciari, G. P. Salam, and G. Soyez, "The Catchment Area of Jets", *JHEP* **0804** (2008) 005, doi:10.1088/1126-6708/2008/04/005, arXiv:0802.1188.

[24] CMS Collaboration, "Tracking and Primary Vertex Results in First 7 TeV Collisions", *CMS-PAS* **TRK-10-005** (2010).

[25] CMS Collaboration, "Tau identification in CMS", *CMS-PAS* **PFT-11-001** (2011).

[26] CMS Collaboration, "Isolated Photon Reconstruction and Identification at sqrts=7 TeV", *CMS-PAS* **EGM-10-006** (2011).

[27] S. Catani, M. Fontannaz, J. P. Guillet et al., "Cross-section of isolated prompt photons in hadron hadron collisions", *JHEP* **05** (2002) 028, arXiv:hep-ph/0204023.

[28] P. Aurenche, M. Fontannaz, J.-P. Guillet et al., "A New critical study of photon production in hadronic collisions", *Phys. Rev.* **D73** (2006) 094007, doi:10.1103/PhysRevD.73.094007, arXiv:hep-ph/0602133.

[29] CMS Collaboration, "Commissioning of b-jet identification with pp collisions at sqrt(s) = 7 TeV", *CMS-PAS* **BTV-10-001** (2010).

[30] A. L. Read, "Presentation of search results: The CL(s) technique", *J. Phys.* **G28** (2002) 2693–2704, doi:10.1088/0954-3899/28/10/313.

[31] G. Cowan, K. Cranmer, E. Gross et al., "Asymptotic formulae for likelihood-based tests of new physics", *Eur. Phys. J.* **C71** (2011) 1554, doi:10.1140/epjc/s10052-011-1554-0, arXiv:1007.1727.

[32] ATLAS and CMS Collaboration, "Procedure for the LHC Higgs boson search combination in Summer 2011",. ATL-PHYS-PUB-2011-11, CMS NOTE-2011/005.

[33] LHC New Physics Working Group Collaboration, "Simplified Models for LHC New Physics Searches", arXiv:1105.2838.